Current Science
CS 5 (1), 1388– 1399 *(2025)*
Received 15 **Dec** 2024 | **Revised 18 Jan** 2025 | **Accepted 15 Feb**. 2025 | **Online Available 28 Feb** 2025
https://doi.org/ 10.52845/CS/2025-5-1-33

Current Science

Current Science

OPEN ACCESS

ISSN(O)2795-8639

ORIGINAL ARTICLE

How to Quickly Identify the Incorporation of Steel Slag in Manufactured Sand?

Tianlei Wang[1], Ziheng Wei[1], Zhang Lei[1*], Xiaoxiao Zhang[1], Changsheng Yue[2*]

[1]School of Materials and Engineering, Tianjin Key Laboratory of Building Green Functional Materials, Tianjin Chengjian University, Tianjin 300384, China

[2]MCC Group, Central Research Institute of Building and Construction Co., Ltd., Beijing 100088, China

[*]Corresponding Author: Zhang Lei, Changsheng Yue

Abstract

In recent years, the quality problem caused by the application of steel slag in concrete buildings have occurred one after another, which has been widely concerned and valued by the construction industry. How to effectively prevent steel slag from being incorporated into the raw materials of concrete has become a major problem. In this paper, the phase composition, chemical composition and macroscopic morphology of steel slags were analyzed in detail to clarify their characteristic identification elements. Subsequently, the rapid identification and detection methods of steel slag mixed in common fine aggregate of concrete were explored by means of grey value analysis, spectral analysis and deep learning. It can be found that the steel slag with high iron content makes the color of particles relatively dark. With the increase of steel slag content maxed in common fine aggregate of concrete, there is a linear positive correlation between the diffuse reflection absorption intensity and the steel slag content in visible light and near-infrared light range, while the grey value shows a decreasing trend with the steel slag content. Compared with the UNet model, the TransUNet model, which introduces a self-attention mechanism, can enhance the global perspective of recognition, thereby significantly improving the recognition accuracy for low content. Therefore, the use of grey value analysis, diffuse absorption spectrum and deep learning image recognition technology can effectively identify whether steel slag is mixed in manufactured sand, so as to ensure the safety and stability of concrete structures.

Keywords: **Steel slag; basic properties; characteristic elements; identification technology**

Introduction

In general, 100~150 kg of steel slag (SS), which is the main industrial by-product in the steelmaking process, is produced for each ton of steel (Jiang, *et al*., 2018; Na, *et al*., 2021). At present, the accumulation amount of SS in China has reached 1 billion tons, resulting in a serious waste of resources and environmental pollution. Therefore, the multi-field and multi-level resource utilization of SS, such as valuable component recovery, cement, concrete, road construction, fertilizer and electrocatalysis, has become a research hotspot in recent years (Martins, *et al*., 2021; Pasetto, *et al*., 2017; Diniz, *et al*., 2017; Wang, *et al*., 2021). Neves, *et al*. (2023) explored the mechanical properties of asphalt mixture with different proportions of SS content (0%, 20% and 35%). With the increase of SS content, the Marshall stability increases linearly. When the SS content was 35%, the stability can reach 16.775 kN. Clay bricks with good performance were successfully prepared by using solid waste such as SS powder, clay brick powder and fly ash. Since the clay brick powder contains porous quartz phase, it can provide space for the hydration expansion of f-CaO, thereby reducing the harm of f-CaO and improving the volume stability of the product. In addition, C_2S and C_3S in SS powder have a fast hydration rate, and a large number of hydration products such as C-S-H gel are formed in the early hydration, thus improving the early compressive strength of clay bricks (Liu, *et al.*, 2024).

Due to the unique chemical composition and mineral composition of SS, it is possible to use it as a substitute for auxiliary cementitious materials, coarse aggregate and fine aggregate in concrete (Fang, *et al.*, 2024; Zhang, *et al.*, 2011; Franco, *et al.*, 2019). The use of low-volume SS instead of coarse aggregate can improve the microstructure of the matrix and gradually increase the compressive strength. However, when the substitution rate exceeds 30%, the tensile strength decreases slightly (Mitwally, *et al.*, 2024). Zhuo, *et al.* (2022) explored the effect of different proportions (0%, 5%, 10%, 15% and 20%) of SS powder as cementitious material on the fracture properties of concrete. Compared with ordinary concrete, when the replacement rate of SS powder was 5%, the fracture energy of SS powder concrete increased by 13.63%, and the fracture toughness increased by 53.22%.

The differences in raw materials, steelmaking process, additives and cooling process of SS lead to great differences in chemical composition and mineral composition of SS particles in different producing areas and different periods (Matsuura, *et al.*, 2022; Dong, *et al.*, 2021; Jiang, *et al.*, 2018). Among them, the f-CaO, f-MgO and other substances often in SS can undergo hydration reaction with water, accompanied by volume expansion, which is a severe test for the safety and stability of concrete products and even buildings. Kuo, *et al.* (2015) added different particle sizes of basic oxygen furnace slag and desulfurization slag into concrete for thermal curing treatment, and observed the effect of each particle size on the volume stability of concrete. When 0.30-0.60 mm and 0.60-1.18 mm SS particles are added, the expansion of the sample is the largest. After 96 h of thermal curing, the volume expansion rate of concrete obtained by replacing different proportions of natural sand with electric arc furnace oxidizing slag can reach 0.13%, which has a certain risk of fracture failure (Kuo, *et al.*, 2014). In addition, waste magnesia-chrome refractory brick particles with different particle sizes and MgO-xFeO-yMnO ternary solid solution particles were used to simulate magnesia expansion particles in SS to investigate the effect of magnesia particles on the volume stability of cement-based materials. With the increase of MgO expansion particle size, the phenomenon of expansion stress concentration and anisotropic expansion in the system show an increasing trend, which has a significant impact on the volume stability of cement-based materials (Long, *et al.*, 2023). Therefore, strictly limiting the application of SS in concrete is a key measure to ensure the quality of concrete engineering.

At present, it can be simply distinguished by the appearance characteristics of SS and common fine aggregate, such as color, shape and morphology. However, with the increasing types of fine aggregates in concrete, the differences in macroscopic characteristics such as color and shape are gradually reduced, and the traditional identification methods based on experience and visual observation cannot effectively distinguish them. Xu, *et al.* (2023) introduced the morphology, microstructure and internal structure of SS by means of optical and electron microscopy, and compared the accuracy and limitations of various methods in determining the mineral composition and chemical composition. Chen, *et al.* (2024) used industrial CT scanning technology to obtain the morphological characteristics of SS particle concrete samples with different contents (3%, 6%, 9%). Compared with other commonly fine aggregates, SS particles with high density have higher brightness under CT scanning, so that the proportion of SS particles in concrete can be quantitatively analyzed through controlling grey value range.

Traditional recognition methods often rely on manual observation and experience to judge, which is not only inefficient, but also susceptible to subjective factors. Deep learning can automatically learn sample features from a large amount of data, and then perform more accurate and efficient classification and identification. It has been widely used in the fields of concrete strength prediction, mix ratio optimization, crack detection and analysis, showing great advantages (Khan, *et al.*, 2022). Sun, *et al.* (2021) used deep learning to detect cracks and bugholes on the surface of concrete. The accuracy of crack detection was up to 97.63%, and the accuracy of bughole detection was 93.53%. Tran, *et al.* (2022)

used three hybrid models of gradient boosting, artificial neural network and random forest combined with particle swarm optimization algorithm to predict the chloride content in concrete, and the accuracy was higher than 90%. Liu, *et al*. (2023) selected the optimal network as the framework to evaluate the dispersion uniformity of SS in asphalt mixture by comparing DeepLabV3+, U-Net and PSPNet networks, and found that the accuracy rate was 96.98%, which provided a new idea for subsequent research. Teng, *et al*. (2023)added the squeezing and excitation attention mechanism in the ConvNeXt model, thereby improving the ability to extract color characteristics of the SS mixture. After using the migration learning training method, the key features of the image can be better obtained, and the prediction accuracy of the model for the SS replacement rate can reach up to 92.64%.

Therefore, this paper systematically studied the chemical composition, mineral composition and macroscopic morphology of SS to explore the relationship between composition-structure-performance, and then clarified the characteristic identification elements. On this basis, the rapid identification technology of SS and common fine aggregate was determined by means of ultraviolet-visible diffuse absorption spectrum, grey value analysis and deep learning, so as to provide certain technical guidance for ensuring the safety and durability of concrete.

1. Experimental details

In this paper, three kinds of SS from different producing areas were selected for comparative analysis. Among them, the first SS (SS-1, the density of 2.92 g/cm^3) was taken from a steel plant in Zhanjiang, Guangdong Province. The second SS (SS-2, the density of 3.51 g/cm^3) was taken from a steel plant in Tangshan City, Hebei Province. The third SS (SS-3, the density of 3.37 g/cm^3) was also taken from another steel plant in Tangshan, Hebei Province. Manufactured sand (MS, the density 2.63 g/cm^3) was selected as the common fine aggregate of concrete, which was purchased in the building materials market. Barium sulfate (spectral purity) was provided by Shanghai Yien Chemical Technology *Co., Ltd*. In order to carry out the subsequent experiment, the samples of SS and MS from three different origins were mixed and recorded as MS@SS-1, MS@SS-2 and MS@SS-3, respectively. According to the volume substitution method, SS from three different origins was evenly mixed with MS at 5%, 10%, 15% and 20%, respectively.

The morphology of the samples was analyzed by ultra-depth-of-field microscope (VHX-600e, KEYENCE Co., Ltd., Japan). The mineral composition of the samples was analyzed by X-ray diffractometer (D/MAX-Ultima IV, Rigaku *Co., Ltd*.). The chemical composition and their contents were determined by X-ray fluorescence spectrometer (ZSXPrimus II, Rigaku *Co., Ltd*.). The diffuse absorption intensity of the samples was measured by UV-Vis-NIR spectrophotometer (LAMBDA750, PerkinElmer), and the test range was 200-2500 nm. Image-J software(1.52a) was used to binarize the sample images and calculate their grey values.

Based on the Windows 11 operating system, the Unet and TranUNet models were built in Python environment for deep learning of SS recognition. Among them, the encoder of UNet first performs three times of downsampling to extract features, and saves the corresponding pre-downsampling feature map as a jump connection. After three times of upsampling, the extracted features were fused with the corresponding size feature maps retained before. The difference between TransUNet and UNet is the encoder part. The feature map after 3 times of downsampling also need to be encoded by the Transformer module. The data set was a self-made SS and MS mixed sample data set under different light conditions and different angles. Each type of SS collected 150 RGB images, including 112 training set, 28 validation set, and 10 test set. Precision , Recall, $F_{1\text{-score}}$ were used as evaluation indexes to measure the detection effect of SS. Precision represents the correct data proportion of the positive samples predicted by the model, and its calculation is shown in Formula (1). Recall represents the proportion of positive samples in the sample that predicts the correct data, and is calculated as shown in Formula (2). $F_{1\text{-score}}$ can comprehensively reflect the accuracy and recall ability of the model, and its calculation is shown in Formula (3). For each type of SS particles, FP represents the number of SS particles that are mistakenly detected, TP represents the number of SS particles that are correctly detected, FN represents the number of SS particles that are missed.

$$Precision=TP/(TP+FP) \quad (1)$$

$$Recall=TP/(TP+FN) \quad (2)$$

$$F_{1\text{-score}}=2/(1/Precision+1/Recall) \quad (3)$$

The images of MS@SS-1 with different contents were collected for the predictive and identification of the presence or absence and exact content of SS. The dataset was 130 images of samples, of which 104 images were used for training set and 26 for validation set. For the test set, 600 images of samples with different contents (0%, 5%, 10%, 15%, 20%, 100%) and different areas of samples were selected, including 100 images for each content. A recognition threshold is set, because the recognition result with SS content of 0% cannot be obtained in this experiment, due to the nature of the samples and the model prediction method. Above this threshold, it is determined that the sample contains SS, and vice versa. Subsequently, the accuracy of the identification results was statistically counted to determine the accuracy of the model identification. In addition, due to the inhomogeneity of SS particles size and the inhomogeneity of local mixing, the two-dimensional images cannot fully reflect the true content of SS. In the content identification work, the allowable error range of MS@SS-1 with SS content of 5%, 10% and 15% is ±2.5%, SS content of 20% is 17.5%-50%, the allowable error range of pure SS content is 50%-100%, whereas the allowable error range of pure MS is 0%-2.5 %, the allowable error range of MS is 0%-2.5%, so as to analyse the effectiveness of deep learning for SS mixed with MS.

3. Results and discussion

As shown in Table 1, the total contents of SiO_2 and Al_2O_3 in MS can reach more than 82%, indicating that it is mainly composed of aluminosilicate minerals. Among them, the content of SiO_2 has the highest percentage of 68.30%, followed by Al_2O_3 with 14.80%. It is particularly noteworthy that the Fe_2O_3 in MS only accounts for 3.64% of the total mass, but all SS from three different sources have higher Fe_2O_3 contents, which can even reach 26.52%, 22%, and 34.9%, respectively. The high CaO content in the SS is 45.8%, 36.4%, 36.6%, which is mainly due to the addition of limestone to achieve the purpose of desulphurisation and dephosphorisation in the process of iron and steel smelting. Meanwhile, magnesium-containing minerals such as dolomite or magnesite are associated in limestone, resulting in MgO contents of 4.85%, 8.79%, and 4.79% in the SS. In addition, compared to MS, SS contains more MnO and less Al_2O_3. In summary, SS contains a large amount of CaO and a high proportion of heavy ferrous elements such as Fe and Mn, while MS has a high percentage of light elements such as Si and Al.

Table 1 The chemical composition of SS and MS from different steel plants (*wt*%)

	CaO	**SiO_2**	**Na_2O**	**Fe_2O_3**	**MgO**	**Al_2O_3**	**MnO**
SS-1	45.80	11.60	0.43	26.52	4.85	3.30	2.83
SS-2	36.40	18.00	0.17	22.00	8.79	5.35	3.98
SS-3	36.60	14.60	0.10	34.90	4.79	2.91	2.31
MS	1.58	68.30	2.41	3.64	0.86	14.80	/

As shown in Fig. 1a, the mineral composition of SS are very complex due to the influence of raw materials, steelmaking process, cooling method and other factors, mainly including C_2S, C_3S, RO phase, calcite, hematite, mayenite, monticellite, fayalite, *etc*. In MS, it is mainly composed of aluminosilicate minerals, including muscovite, quartz and potassium feldspar. Among them, the Fe element with higher content in SS mainly exists in the form of hematite, and calcium mainly exists in minerals such as C_2S, C_3S, calcite and monticellite olivine. Therefore, light-coloured minerals such as quartz, potassium feldspar and other aluminosilicate minerals are dominant in MS, while SS contains dark-coloured minerals such as hematite, *etc*. The difference of mineral composition between SS and MS leads to obvious color change, which lays a theoretical foundation for the rapid identification of SS and MS mixture.

Due to the gas escape phenomenon during the cooling process of SS particles, the SS particles are porous (Fig. 1b,c,d,e). MS is mostly obtained from mechanical crushing of tailings and waste rock, so its particle surface is relatively dense and the edges and corners are more distinct. Due to the high Fe element content in SS, the particles are darker in colour; whereas MS has a higher content of Si and Al elements, and the particles are lighter in colour. However, MS also contains a small amount of dark-coloured particles, which is mainly due to the enrichment of dark-coloured minerals inside the particles.

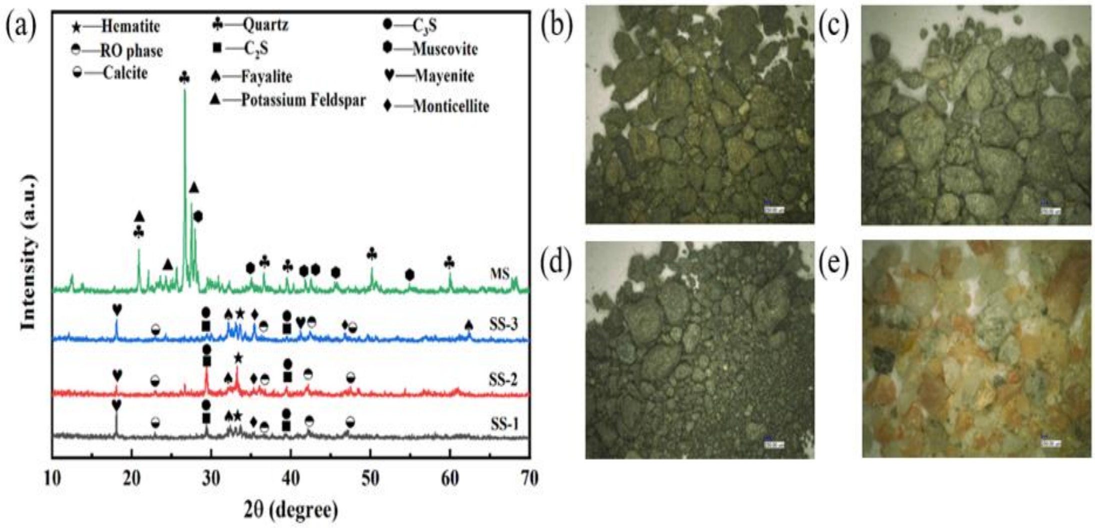

Figure 1 Mineral composition of SS and MS from different steel plants(a) and super depth of field photographs of SS and MS from different steel plants
(b: SS-1, c: SS-2, d: SS-3, e: MS)

As can be seen in Fig. 2a, the diffuse absorption intensity of the mixed samples of MS@SS-1 increases gradually with the increase of the content. In the UV interval, the diffuse absorption intensity of pure SS-1 is the largest, but the absorption intensity does not show a clear regularity with the content of SS-1. In the visible light interval, the mixed samples shows no obvious characteristic absorption peaks. After extracting the absorption intensities at 585.0 nm for different contents, the fitting coefficient (R-square) obtained by linear fitting is 0.97, showing a good linear relationship (Fig. 2b). An increase in the number of absorption peaks on the curve is observed in the near-infrared light region. By fitting the absorption intensities at 840.0 nm and 1415.0 nm, an R-square of 0.96 and 0.93 is obtained, respectively, showing a certain linear trend (Fig. 2c, d).

As can be seen in Fig. 2e, the absorption intensity of the mixed samples of MS@SS-2 is gradually enhanced with the increase of SS-2 content. In the UV range, the samples do not show a clear pattern between the absorption intensity and the contents. In contrast, in the visible and near-infrared ranges, the R-square is 0.97, 0.99 and 0.94 when the absorption intensities at 585.0 nm, 840.0 nm, and 1415.0 nm are fitted to the content, respectively, showing a good linear relationship. Therefore, MS@SS-2 is more suitable for effective identification by detecting the absorption intensity in the visible and near-infrared regions.

Similarly, it can be seen from Fig. 2i that the absorption intensity of MS@SS-3 increases gradually with the increase in the content. The absorption intensities at the points of 585.0 nm, 840.0 nm, and 1415.0 nm are selected to be fitted with the content, and their R-squares are 0.97, 0.96, and 0.91, respectively, which shows an obvious linear relationship. In conclusion, detecting the absorption intensities at 585.0 nm, 840.0 nm, and 1415.0 nm in the visible and near-infrared light intervals can provide an effective identification of the content of SS mixed in MS.

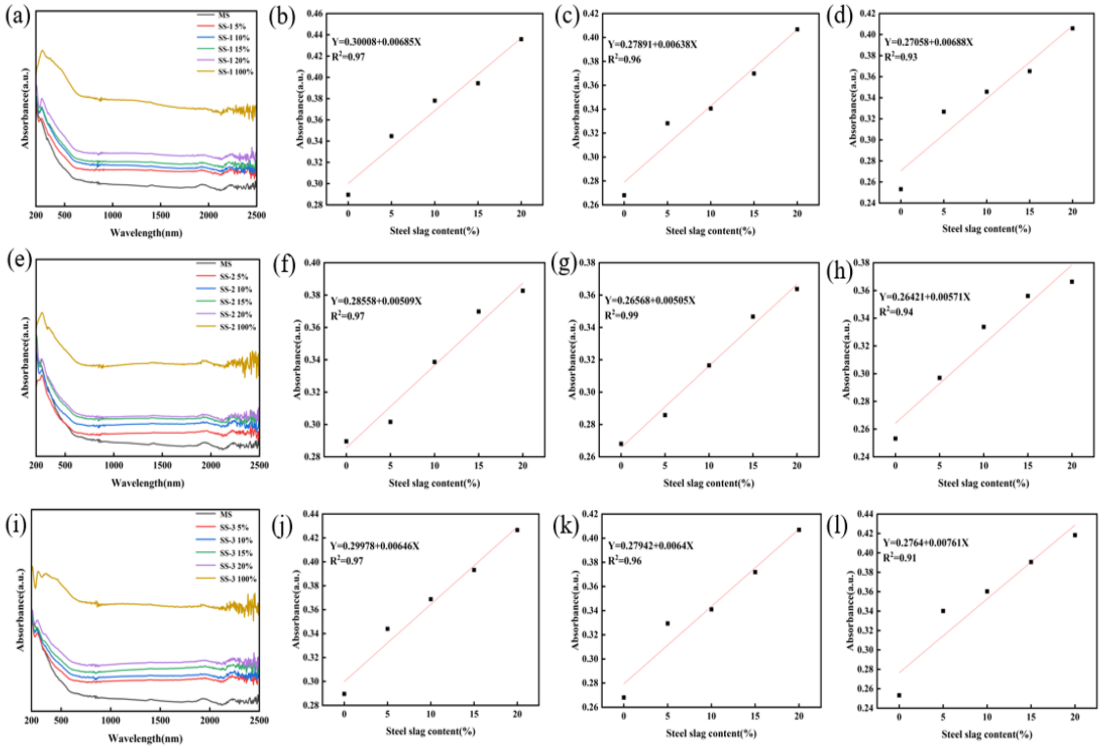

Figure 2 Diffuse absorption spectrum of MS@SS-1,SS-2,SS-3 with different contents (a,e,i) and linear relationship between SS-1 content and its absorption intensity at 585.0 nm (b,f,j), 840.0 nm (c,g,k), 1415.0 nm (d,h,l)

The super depth of field microscope photographs of SS and MS from different steel plants and their grey value analysis are shown in Fig. 3a,b,c,d. The Fe_2O_3 content in SS-1, SS-2, and SS-3 is higher with 26.52%, 22.00%, and 34.90%, respectively, which makes more ferrous minerals inside the particles, and consequently leads to darker colour of the SS. After binarization of the photographs, the main peak positions of the grey values (Mode values) of the three SS are 55, 92 and 62, respectively, while MS has less iron content and is mainly dominated by aluminosilicate minerals, so its particles are lighter in colour, with a Mode value as high as 145. It can be seen that the differences in the chemical and mineral composition directly affect the colour of the particles, which leads to significant differences in the grey values of the photographs.

The dark particles in the photographs gradually increases with the increase of the SS content (Fig. 3e,f,g,h). The grey value analysis reveals that when the content is 5%, the Mode value of the photographs is 124, which was reduced by 18 as compared to the pure MS grey value. The Mode value of the SS-1 content is 115, 106, and 102 for the content of 10%, 15% and 20% respectively. It can be seen that with the increase in the content of SS-1, the number of dark-color particles in the field of view increases, thereby gradually decreasing the overall grey value of the image.

SS-2 contains more Fe and Mn elements, whereas MS has a higher content of Si and Al elements, resulting in a significant colour difference between the particles of the two (Fig. 3i,j,k,l). When the content of SS-2 was increased from 5% to 20%, the number of dark particles in the image gradually increased, and the Mode values decreased to 121, 115, 106 and 100 in turn, thus indicating an inverse relationship between the SS-2 content and the grey value.

Similarly, the change in SS-3 content directly affects the grey values of the mixed samples' photographs taken under the super depth of field microscope. With the increase of SS-3 content(5%, 10%, 15% and 20%), the Mode values gradually decrease to 126, 120, 114, and 105, indicating that the SS-3 content is negatively correlated with the grey value (Fig. 3m,n,o,p). Therefore, it is possible to identify whether there is SS mixing in MS by analyzing the grey value of the sample photographs.

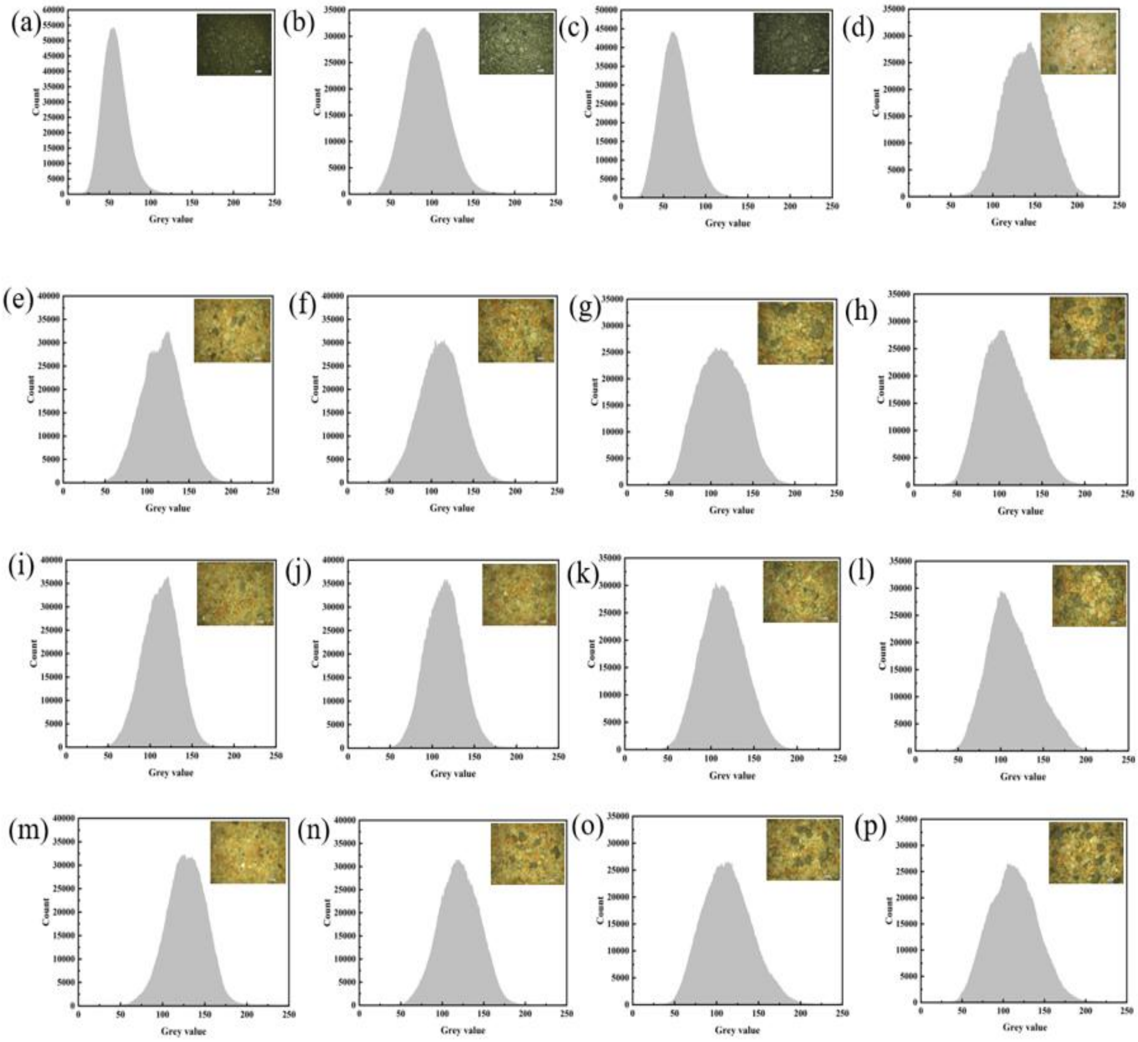

Figure 3 Super depth of field microscope photographs and the grey value analysis of SS and MS (a : SS-1, b,: SS-2, c: SS-3, d: MS) and super depth of field microscope photographs and the grey value analysis of MS@SS-1,SS-2,SS-3 (e,i,m : 5%、f,j,n: 10% ,g,k,o : 15% ,h,l,p : 20%)

Based on the feature differences between SS and MS particles, especially the colour characteristics, traditional detection methods such as diffuse absorption spectrum and the grey value analysis of photographs can be used to achieve effective recognition between SS and MS. However, the operation process of traditional detection methods is relatively cumbersome, and the recognition accuracy is easily affected by the environment and the quality of the samples. Therefore, deep learning is intended to perform image segmentation and recognition on samples. Fig.4 shows the original photographs of SS and MS from some different producing plants in the same field of view and their recognition results by UNet and TransUNet model. When the photographs are recognised using the UNet model, there are two categories on single particles, *i.e.*, some regions on SS particles are misclassified as MS particles, while some regions on MS particles are identified as MS particles. This is mainly due to the fact that the UNet model only uses convolutional neural network, which does not have the ability to establish long distance dependencies and cannot take a global view. When the Transformer module is introduced into the UNet model, a self-attention mechanism is added to the model, which reduces the phenomenon that several pixels in a category area are incorrectly predicted as other categories, thereby improving its recognition efficiency.

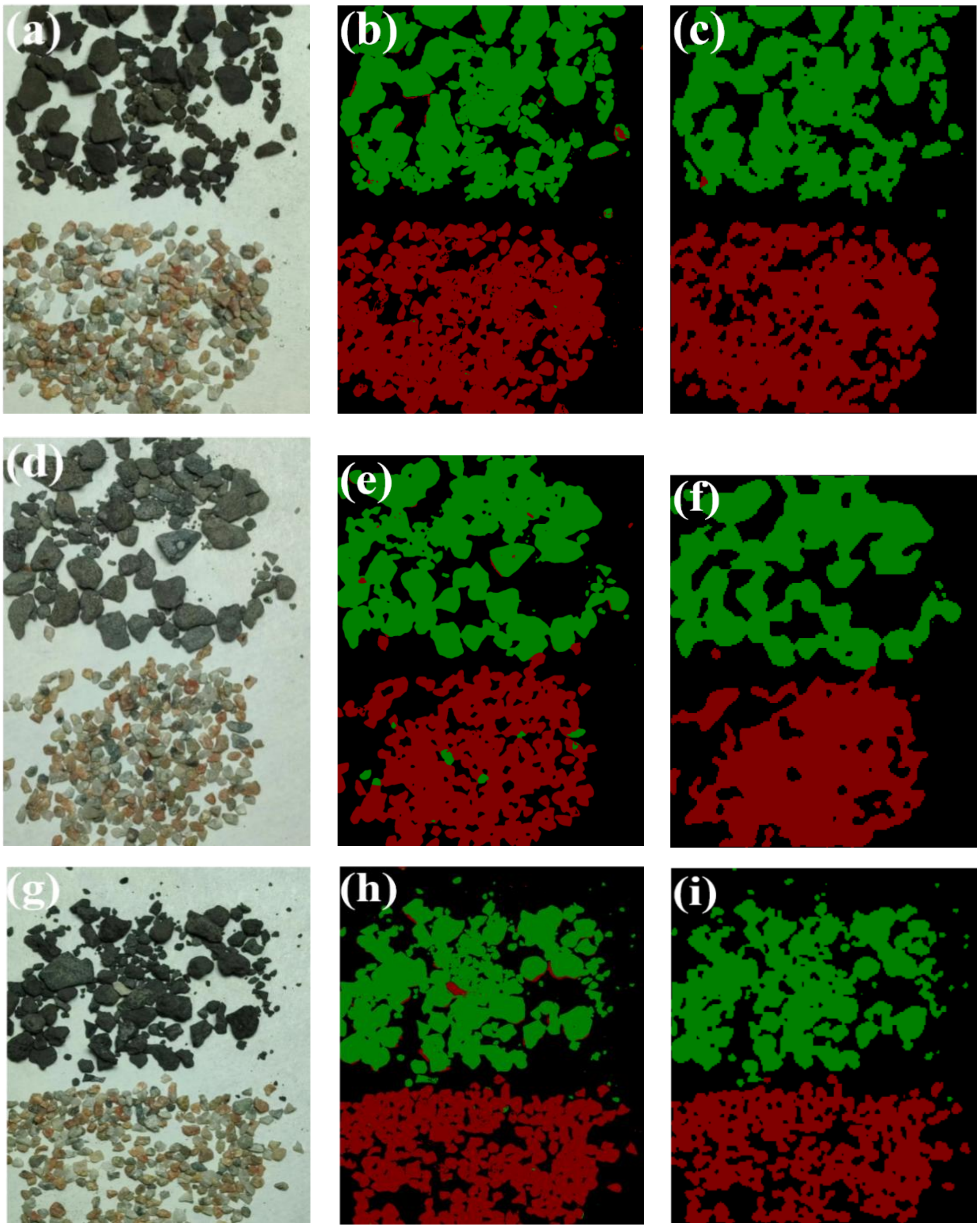

Figure 4 Comparison of the SS and MS's original photographs from different steel plants and their recognition results by deep learning of UNet and TransUNet models (a, b,c: SS-1, d, e,f: SS-2, g, h,i: SS-3)

As shown in Table 2, the precision and recall of the UNet model for MS@SS-1 are 95.3% and 94.6% respectively, indicating that the UNet model can accurately identify MS@SS-1. The precision and recall rates of the TransUNet model with the Transformer module for the same test set are not much different from those of the UNet model, being 95.1% and 94.8%, respectively. When the photographs of MS@SS-2 are put into the UNet model, the precision and recall rates are 87.2% and 86.4% respectively, while the precision and recall rate of the TransUNet model can be improved to 91.9% and 91.6% respectively, which are 4.7% and 5.2% higher than those of UNet model. However, the precision and recall rate of the photographs of MS@SS-3 are 93.5% and 91.7% in the UNet model, and the precision and recall rate are 92.9% and 92.0% in the TransUNet model. The chemical and mineral compositions of SS from different producing areas vary, as do their colours and morphologies, resulting in significant differences in their detectability. However, compared with the UNet model, the TransUNet model with the introduction of the Tranformer module is more stable, with a precision and recall rate of more than 90.0%.

Table 2 The recognition effects of the photographs of SS and MS by UNet model and TransUNet model deep learning

Type of SS	Model	Precision (%)	Recall (%)	$F_{1\text{-score}}$
SS-1	UNet	95.3	94.6	95.0
	TransUNet	95.1	94.8	95.0
SS-2	UNet	87.2	86.4	86.8
	TransUNet	91.9	91.6	91.8
SS-3	UNet	93.5	91.7	92.6
	TransUNet	92.9	92.0	92.5

Due to the poor volume stability of SS particles, their use in concrete products is prone to local bursting point damage, cracking and other phenomena, so it is strictly prohibited to incorporate SS particles into aggregates. With the increasing of the recognition threshold, the recognition accuracy of MS@SS-1 photographs with different contents using UNet model and TransUNet model showed an increasing and then decreasing trend (Fig. 5). The increase of the recognition threshold can reduce the interference of dark particles in MS on the SS recognition results, which makes its recognition accuracy gradually increase. However, when the threshold value is gradually close to 5%, some photographs of the MS@SS-1 with 5% content may be judged as no SS in sample, resulting in a decrease in recognition accuracy. The UNet model is used to recognize the photographs of MS@SS-1, and the recognition accuracy can reach 93.17% at a threshold of 4.5%. However, the TransUNet model has a recognition accuracy of up to 94.67% at a recognition threshold of 3.7%. Therefore, compared with the UNet model, the TransUNet model has a significant decrease in the recognition threshold for whether SS-1 is mixed in MS, thus achieving a more accurate recognition judgement.

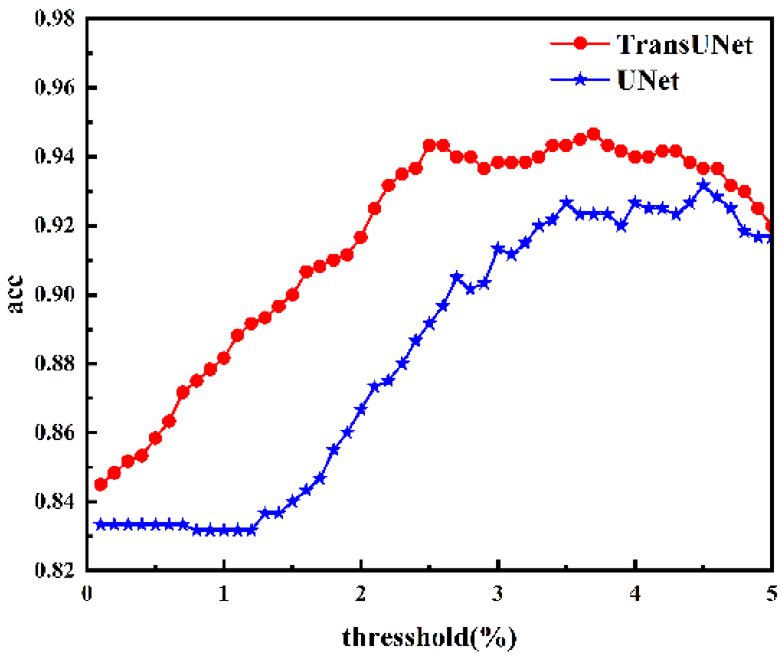

Figure 5 Recognition accuracy of MS@SS-1 photographs using UNet model, TransUNet model under different thresholds

Fig. 6 shows the confusion matrix of MS@SS-1 recognition accuracy using UNet model and TransUNet model. Where the diagonal position is the proportion of correct results predicted by the model, the darker the colour of the square, the more correctly predicted photographs are indicated. The recognition accuracy of UNet model for MS@SS-1 photographs with 0%, 5%, 10%, 15%, 20%, and 100% content is 38%, 48%, 46%, 28%, 22%, and 100%, respectively. Similarly, the recognition accuracy of MS@SS-1 photographs using TransUNet model is 73%, 40%, 44%, 31%, 28%, and 100%, respectively. It can be found by comparison that the recognition error interval set at 100% content is larger, resulting in the best recognition accuracy for both models. However, due to the three-dimensional structure of the particles and the dispersion of SS-1 in MS at low content, it is difficult for the planar image to fully reflect its true content, and the two models are ineffective for the identification of samples with lower content. In addition, the presence of dark-coloured minerals in MS results in darker particles, which can be easily misclassified as SS-1 in the UNet model, while the TransUNet model with the introduction of the self-attention mechanism enhances the global perspective of the identification, which leads to a significant increase in the accuracy of the identification of low-doped samples.

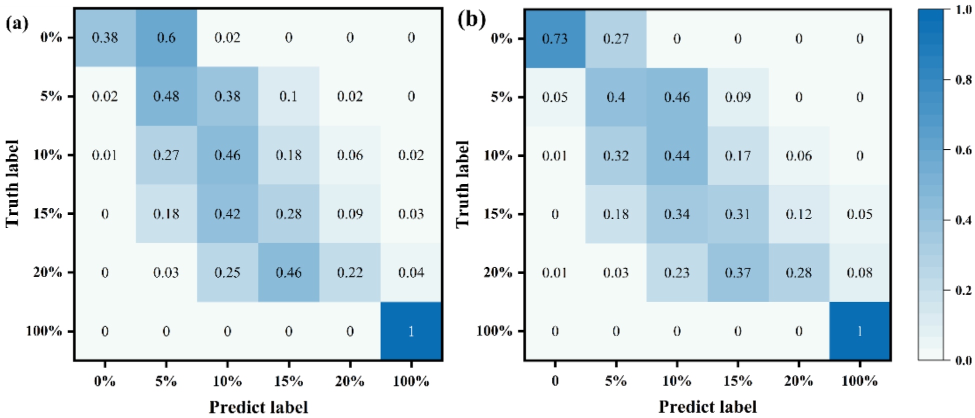

Figure 6 Confusion matrix for recognition accuracy of MS@SS-1 photographs with different contents using UNet model (a), TransUNet model (b)

Conclusion

By comparing the physical composition, chemical composition and macroscopic morphology of SS from different producing areas and MS, it was found that SS have higher content of heavy ferrous elements such as Fe and Mn and is endowed with minerals such as magnetite, which leads to a significant difference in the colour of the particles from most of the MS particles. Therefore, due to the change of chemical composition and mineral composition, which leads to the obvious difference in the colour of SS and MS particles, the color difference of particles is obvious, which can be used as the characteristic identification element between SS and MS. Based on the colour difference characteristics, through the analysis of diffuse absorption spectrum and grey value, it is found that with the increase of SS content, the absorption intensity gradually increases and the grey value gradually decreases. Through deep learning analysis, the TransUNet model has a higher recognition accuracy for SS mixed with MS sample photographs. When the recognition threshold is set to 3.7%, its recognition accuracy is as high as 94.67%. Therefore, this paper clarifies the feature recognition elements between SS and MS, and determines the feasibility of its rapid identification technique through a series of characterisation, so as to provide some technical guidance to ensure the safety and durability of concrete.

Acknowledgements

This study was partially supported by the National Natural Science Foundation of China (Grant Nos. 52078321, 52178265 and 52178264).

Conflicts of Interest

The authors declare that the research was conducted in the absence of any commercial or financial relationships that could be construed as a potential conflict of interest.

Reference

1. Chen C, Li Z H, Pav W X, *et al*. Application of industrial CT to identify mixed steel slag particles in concrete[J]. Journal of Building Materials, 2024, 27(04): 343-349. (in Chinese)
2. Diniz D H, de Carvalho J M F, Mendes J C, *et al*. Blast oxygen furnace slag as chemical soil stabilizer for use in roads[J]. Journal of

materials in civil engineering, 2017, 29(9): 04017118.
3. Dong Q, Wang G, Chen X, *et al*. Recycling of steel slag aggregate in portland cement concrete: An overview[J]. Journal of cleaner production, 2021, 282: 124447.
4. Fang Y, Shan J, Wang Q, *et al*. Semi-dry and aqueous carbonation of steel slag: Characteristics and properties of steel slag as supplementary cementitious materials[J]. Construction and Building Materials, 2024, 425: 135981.
5. Franco de Carvalho J M, Campos P A M, Defáveri K, *et al*. Low environmental impact cement produced entirely from industrial and mining waste[J]. Journal of Materials in Civil Engineering, 2019, 31(2): 04018391.
6. Jiang Y, Ling T C, Shi C, *et al*. Characteristics of steel slags and their use in cement and concrete-A review[J]. Resources, Conservation and Recycling, 2018, 136: 187-197.
7. Jiang Y, Ling T C, Shi C, *et al*. Characteristics of steel slags and their use in cement and concrete-A review[J]. Resources, Conservation and Recycling, 2018, 136: 187-197.
8. Khan K, Ahmad W, Amin M N, *et al*. A systematic review of the research development on the application of machine learning for concrete[J]. Materials, 2022, 15(13): 4512.
9. Kuo W T, Shu C Y, Han Y W. Electric arc furnace oxidizing slag mortar with volume stability for rapid detection[J]. Construction and Building Materials, 2014, 53: 635-641.
10. Kuo W T. Expansion behavior of concrete containing different steel slag aggregate sizes under heat curing[J]. Computers and Concrete, An International Journal, 2015, 16(3): 487-502.
11. Liu J, Yuan L, Wang Z, *et al*. A new method for evaluating the uniformity of steel slag distribution in steel slag asphalt mixture based on deep learning[J]. Construction and Building Materials, 2023, 400: 132766.
12. Liu Y X, Gu F, Zhou H, *et al*. Study on the performance and reaction mechanism of alkali-activated clay brick with steel slag and fly ash[J]. Construction and Building Materials, 2024, 411: 134406.
13. Long Q, Zhao Q, Gong W, *et al*. Effect of magnesian-expansive components in steel slag on the volume stability of cement-based materials[J]. Materials, 2023, 16(13): 4675.
14. Martins A C P, De Carvalho J M F, Costa L C B, *et al*. Steel slags in cement-based composites: An ultimate review on characterization, applications and performance [J]. Construction and Building Materials, 2021, 291: 123265.
15. Matsuura H, Yang X, Li G, *et al*. Recycling of ironmaking and steelmaking slags in Japan and China[J]. International Journal of Minerals, Metallurgy and Materials, 2022, 29 (4): 739-749.
16. Mitwally M E, Elnemr A, Shash A, *et al*. Utilization of steel slag as partial replacement for coarse aggregate in concrete[J]. Innovative Infrastructure Solutions, 2024, 9(5): 1-8.
17. Na H, Wang YJ, Zhang X, *et al*. Hydration activity and carbonation characteristics of dicalcium silicate in steel slag: A Review[J]. Metals, 2021, 11(10): 1580-1596.
18. Neves J, Crucho J. Performance Evaluation of Steel Slag Asphalt Mixtures for Sustainable Road Pavement Rehabilitation[J]. Applied Sciences, 2023, 13(9): 5716.
19. Pasetto M, Baliello A, Giacomello G, *et al*. Sustainable solutions for road pavements: A multi-scale characterization of warm mix asphalts containing steel slags[J]. Journal of Cleaner Production, 2017, 166: 835-843.
20. Sun Y, Yang Y, Yao G, *et al*. Autonomous crack and bughole detection for concrete surface image based on deep learning[J]. IEEE access, 2021, 9: 85709-85720.
21. Teng S, Zhu L, Li Y, *et al*. ConvNeXt steel slag sand substitution rate detection method incorporating attention mechanism[J]. Scientific Reports, 2023, 13(1): 10593.
22. Tran V Q, Giap V L, Vu D P, *et al*. Application of machine learning technique for predicting and evaluating chloride ingress in concrete[J]. Frontiers of Structural and Civil Engineering, 2022, 16(9): 1153-1169.
23. Wang F P, Liu T J, Cai S, *et al*. A review of modified steel slag application in catalytic pyrolysis, organic degradation, electrocatalysis, photocatalysis, transesterification and carbon capture and storage[J]. Applied Sciences, 2021, 11(10): 4539.
24. Xu Y, Lv Y, Qian C. Comprehensive multiphase visualization of steel slag and related research in cement: Detection technology and application[J]. Construction

and Building Materials, 2023, 386: 131572.

25. Zhang T, Yu Q, Wei J, *et al*. Preparation of high performance blended cements and reclamation of iron concentrate from basic oxygen furnace steel slag[J]. Resources, Conservation and Recycling, 2011, 56(1): 48-55.
26. Zhuo K X, Liu G T, Lan X W, *et al*. Fracture behavior of steel slag powder-cement-based concrete with different steel-slag-powder replacement ratios[J]. Materials, 2022, 15(6): 2243.